Linking flood frequency to long-term water balance: Incorporating effects of seasonality

M. Sivapalan,[1] G. Blöschl, R. Merz, and D. Gutknecht

Institute for Hydraulic and Water Resources Engineering, Vienna University of Technology, Vienna, Austria

Received 24 June 2004; revised 4 February 2005; accepted 22 March 2005; published 18 June 2005.

[1] Derived flood frequency models can be used to study climate and land use change effects on the flood frequency curve. Intra-annual (i.e., within year) climate variability strongly impacts upon the flood frequency characteristics in two ways: in a direct way through the seasonal variability of storm characteristics and indirectly through the seasonality of rainfall and evapotranspiration which then affect the antecedent catchment conditions for individual storm events. In this paper we propose a quasi-analytical derived flood frequency model that is able to account for both types of seasonalities. The model treats individual events separately. It consists of a rainfall model with seasonally varying parameters. Increased flood peaks, as compared to block rainfall, due to random within-storm rainfall time patterns are represented by a factor that is a function of the ratio of storm duration and catchment response time. Event runoff coefficients are allowed to vary seasonally and include a random component. Their statistical characteristics are derived from long-term water balance simulations. The components of the derived flood frequency model are integrated in probability space to derive monthly flood frequency curves. These are then combined into annual flood frequency curves. Comparisons with Monte Carlo simulations using parameters that are typical of Austrian catchments indicate that the approximations used here are appropriate. We perform sensitivity analyses to explore the effects of the interaction of rainfall and antecedent soil moisture seasonalities on the flood frequency curve. When the two seasonalities are in phase, there is resonance, which increases the flood frequency curve dramatically. We are also able to isolate the contributions of individual months to the annual flood frequency curve. Monthly flood frequency curves cross over for the parameters chosen here, as extreme floods tend to mainly occur in summer while less extreme floods may occur throughout the year.

Citation: Sivapalan, M., G. Blöschl, R. Merz, and D. Gutknecht (2005), Linking flood frequency to long-term water balance: Incorporating effects of seasonality, *Water Resour. Res.*, *41*, W06012, doi:10.1029/2004WR003439.

1. Introduction

[2] Floods are often generated by different processes in the same catchment. In parts of Western Australia, for example, floods with a return period less than 10 years are typically winter floods, whereas floods with a return period larger than 30 years tend to be summer floods despite generally drier soils in summer [*Sivandran*, 2002]. This arises due to different mechanisms of rain producing events (frontal events in winter, thunderstorms and tropical cyclones in summer), and their interaction with different flooding processes dominating in different times of the year. In Austria there also exist significant seasonal patterns of flood processes. In most of the country, the most extreme floods are summer floods, often produced by long-duration synoptic events, while smaller floods can occur throughout the year [*Merz and Blöschl*, 2003]. Differences in flood processes related to rain-fed (in summer and autumn) and snowmelt driven (spring) floods have received attention in North America and Europe [*Waylen and Woo*, 1982; *Stedinger et al.*, 1992]. *Hirschboeck* [1987] performed a detailed analysis on causative mechanisms of floods in a number of catchments in Arizona based on surface and upper weather maps [*Hirschboeck*, 1988]. This scheme was updated by *House and Hirschboeck* [1997] and simplified into three event types (tropical, convective, and frontal events). The body of work on causative mechanisms allowed *Hirschboeck* [1987] and *Alila and Mtiraoui* [2002] to examine the flood statistics for each group of events and derive hydroclimatically defined mixed distributions in flood series. *Merz and Blöschl* [2003] found significantly different flood frequency statistics for long-rain floods, short-rain floods, flash floods, rain-on-snow floods, and snowmelt floods in Austria. The need to distinguish between flood frequency curves in different months of the year, e.g., between summer and winter, or between rain-fed or snowmelt driven floods, is becoming much more critical because changes in climate and land use cannot be fully investigated without explicitly incorporating changes in the associated intra-annual (e.g., seasonal) and

[1] On leave from Centre for Water Research, Department of Environmental Engineering, University of Western Australia, Crawley, Western Australia, Australia.

0043-1397/05/2004WR003439$09.00

interannual (i.e., between year) variabilities. This is the main motivation for this paper.

[3] Traditional flood frequency analysis depends upon the existence of long periods of flood records. A recent concern with such data-driven procedures is that changes in climate and/or land uses may affect the flood frequencies, yet may not be reflected by the short records we currently have [*Franks and Kuczera*, 2002; *Sankarasubramanian and Lall*, 2003], and the consequent nonstationarities in the data record may invalidate traditional flood frequency analysis. Also, unraveling land use and climate change effects from observed flood frequency curves is notoriously difficult [*Kundzewicz*, 2003].

[4] Therefore flood frequency estimation in the future is increasingly likely to be based on a combination of traditional data-driven procedures, with increased use of rainfall-runoff models that can capture the effects of both climate and land use changes [*Blazkova and Beven*, 1997]. Derived flood frequency procedures are amenable to this kind of investigation. The derived flood frequency approach consists of the following elements: (1) a statistical model of rainfall, usually expressed in the form of a joint probability distribution of rainfall intensity and duration, including, if necessary, a correction for the effects of catchment size; (2) a deterministic rainfall-runoff model which, in turn, contains three components, namely, a runoff generation model, a runoff routing model, and a method for the accounting of antecedent catchment wetness; and (3) a mathematical framework, or "methodology", within which the above two elements are combined together to permit the "derivation" or estimation of the probability of exceedance of a given flood magnitude, thus leading to the "derived" flood frequency curve. In previous work two alternative methodologies have been adopted for deriving the flood frequency curve. The first approach is a Monte Carlo approach where rainfall time series are generated by a stochastic rainfall model and used to drive a continuous rainfall-runoff model [*Ott and Linsley*, 1972; *Beven*, 1986; *Rahman et al.*, 2002]. From the runoff time series so generated the flood frequency curve is constructed. The second approach is a direct or analytical approach where the flood frequency curve is derived from the rainfall frequency curve using derived distribution theory [*Eagleson*, 1972; *Sivapalan et al.*, 1990; *Fiorentino and Iacobellis*, 2001]. It is only feasible when the rainfall-runoff model and the stochastic models of rainfall and antecedent conditions are simple enough for the derivations to be analytically tractable but has the advantage that the effects of the various processes can be clearly distinguished in the final set of equations. The main contribution of the derived flood frequency approach has been the ability to understand the process controls of flood frequency behavior, especially the ability to focus attention on change of dominant processes with increasing return period [*Sivapalan et al.*, 1990; *Blöschl and Sivapalan*, 1997], and therefore the ability to adapt flood estimation procedures to these dominant processes [*Jothityangkoon and Sivapalan*, 2001].

[5] Intra-annual variability in climate impacts upon the flood frequency curves in two ways: (1) seasonal and interannual variability of storm characteristics have a direct bearing on flood frequency distributions and (2) seasonality of rainfall and evapotranspiration affect the antecedent catchment conditions for individual storm events, and thus have an indirect effect on the magnitudes of the flood peaks. In spite of the widely acknowledged importance of seasonality of storm characteristics and of antecedent conditions on flood frequency these effects, to our knowledge, have never been explicitly included in any of the analytical derived flood frequency models presented in the literature. Clearly, this requires an explicit linking of derived flood frequency models with long-term water balance models, around a mathematical framework that enables the explicit inclusion of seasonality. This is the subject matter of this paper. Specifically, the aim of this paper is to explore the connection between the seasonality of floods and the seasonalities of climatic characteristics and the catchment state.

[6] The presentation of the paper will adopt the following outline. In section 2 we give examples of seasonal variability of flood frequency. We then give a mathematical presentation of the quasi-analytical derived flood frequency methodology in section 3, including a description of the way we derive annual flood frequency curves from monthly curves. In section 4 we describe the implementation of the continuous simulation or Monte Carlo approach with the same or equivalent model structures and parameters as the quasi-analytical approach, which we will use as a check of the quasi-analytical results. Section 5 is devoted to the application of the new derived flood frequency methodology to a typical catchment in Austria, its validation by comparing against results obtained using the Monte Carlo simulation approach, and the use of sensitivity analysis to gain insights into the effects of seasonality on monthly and annual flood frequency curves. Section 6 provides a discussion and the conclusions.

2. Examples of Seasonal Variability of Flood Frequency

[7] To further motivate the use of derived flood frequency models that represent the seasonalities of climate and soil moisture we illustrate the importance of seasonality through a number of examples taken from Austrian catchments. These examples also assist in guiding the development of our generalized flood frequency method.

[8] Figure 1 presents, for four Austrian catchments, plots of the month in which the annual maximum flood occurred for each year of record against the estimated return period for that flood. In the Teufelmühle catchment (Figure 1a) located in the north of Austria, we note that at low return periods the annual maximum floods could occur in any of the 12 months in a fairly uniform manner, whereas with increasing return period, the annual maximum floods tend to be produced preferentially in the December to March (winter) period. On the other hand, in the Wienerbruck catchment (Figure 1b) located in the Alps, there is a similar narrowing down in the timing of annual maximum floods with increasing return period, but this time around the July to September (summer) period. In the Anger catchment (Figure 1c) located in southeastern Austria, there is not the same degree of narrowing down in the timing of floods, with most floods occurring in the May to October period, regardless of return period. Finally, in the Rattendorf catchment (Figure 1d) located in southern Austria, the

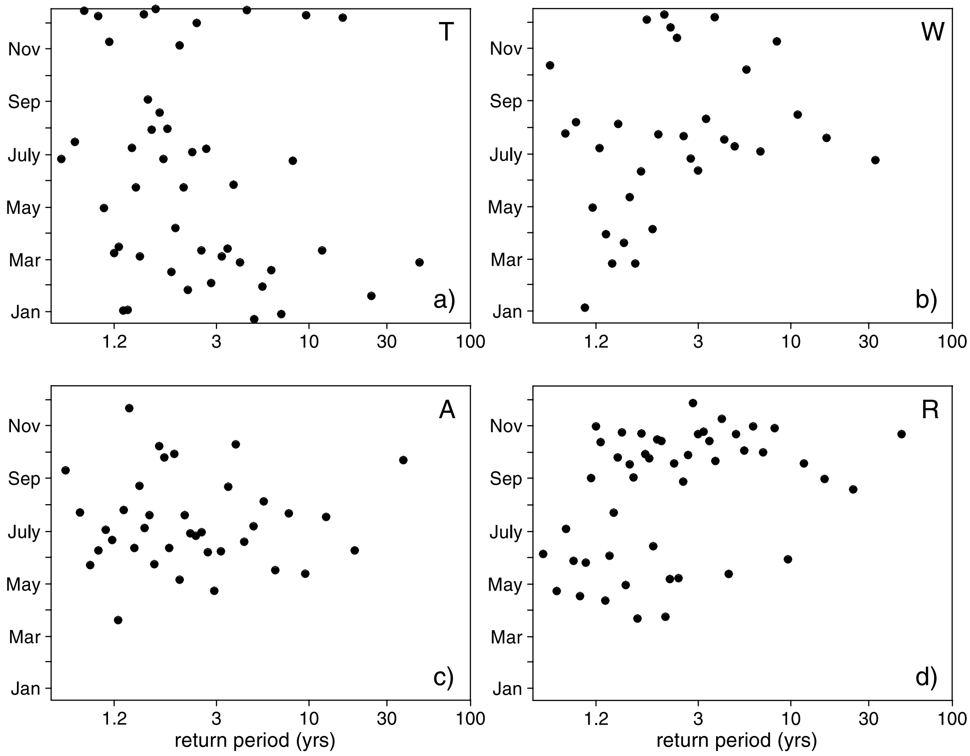

Figure 1. Seasonality of flood frequency (date versus return period) for four example catchments in Austria: (a) Teufelmühle, (b) Wienerbruck, (c) Anger, and (d) Rattendorf. The mean catchment elevations and catchment areas are Teufelmühle, 751 m, 452 km^2; Wienerbruck, 1013 m, 36 km^2; Anger, 994 m, 408 km^2; Rattendorf, 1380 m, 595 km^2.

narrowing down in the timing of annual maximum floods shows a rather bimodal variation, with one set of floods occurring preferentially around June (spring) and the next around October (early winter). Clearly, these observed patterns must have both hydrological causes, and hydrological consequences, and yet analyses of these are precluded in traditional flood frequency analysis.

[9] We can speculate on possible physical causes of the observed seasonality in the timing of annual maximum flood peaks. Strong seasonal contrast in a number of contributing factors can have a significant effect on the extremes: rainfall, snowmelt, the underlying water balance reflected in the runoff coefficient and initial base flow in the streams. The first obvious cause could be the seasonality of rainfall inputs, especially the seasonality of extreme (flood producing) storms. Figure 2 presents the number of "extreme storms" as a function of the month for four regions in Austria that are loosely associated with the catchments of Figure 1 described above: Figure 2a shows Moldau (Teufelmühle), Figure 2b shows Donau between Enns and March (Wienerbruck), Figure 2c shows Raab (Anger), and Figure 2d shows Drau (Rattendorf). These were taken from *Gutknecht and Watzinger* [1996], where "extreme storms" are defined as those storms that have the property that d $>\sqrt{5t_r}$, where t_r is rainfall duration in minutes and d is the total rainfall depth in mm over this duration. In the case of the Drau region and the associated Rattendorf catchment, presented in Figures 2d and 1d, the close association between the bimodal distribution of the timing of annual maximum floods (June and October) and the similarly bimodal distribution of extreme storms is unmistakable, and therefore the seasonality of extreme storms must be a primary determinant of seasonality of floods. In the Donau between Enns and March region and the Wienerbruck catchment, presented in Figures 2b and 1b, the most extreme storms appear to occur in summer which seems to be reflected also in the timing of annual maximum floods. The same appears to hold for the Raab region and the Anger catchment, where the extreme storms are mainly centered around June (Figure 2c) and the timing of annual maxima floods directly follow (Figure 1c). However, in the Moldau region and the Teufelmühle catchment the temporal distribution of extreme storms tends to be centered around July (Figure 2a), and yet annual maximum floods tend to be strongly centered around January at large return periods (Figure 1a). At least in the latter case, the observed seasonality is not directly attributable to seasonality of extreme storms. We must therefore seek alternative or additional explanations.

[10] Figure 3 presents the seasonal (monthly) variation of the runoff coefficient at event scale and the base flow for the four Austrian catchments considered before. In Figure 3a the base flow is defined as the minimum of daily runoff in each month, averaged over 30 years. Minimum runoff is an indicator of low flow and has here been used as a proxy for base flow. In Figure 3b the runoff coefficient has been estimated through the application of a variant of the HBV model [*Merz and Blöschl*, 2003, 2004] and is defined as the direct runoff divided by the sum of rainfall and melt input, averaged over each month and averaged over 30 years of record (thick lines). The thin lines in Figure 3b show the

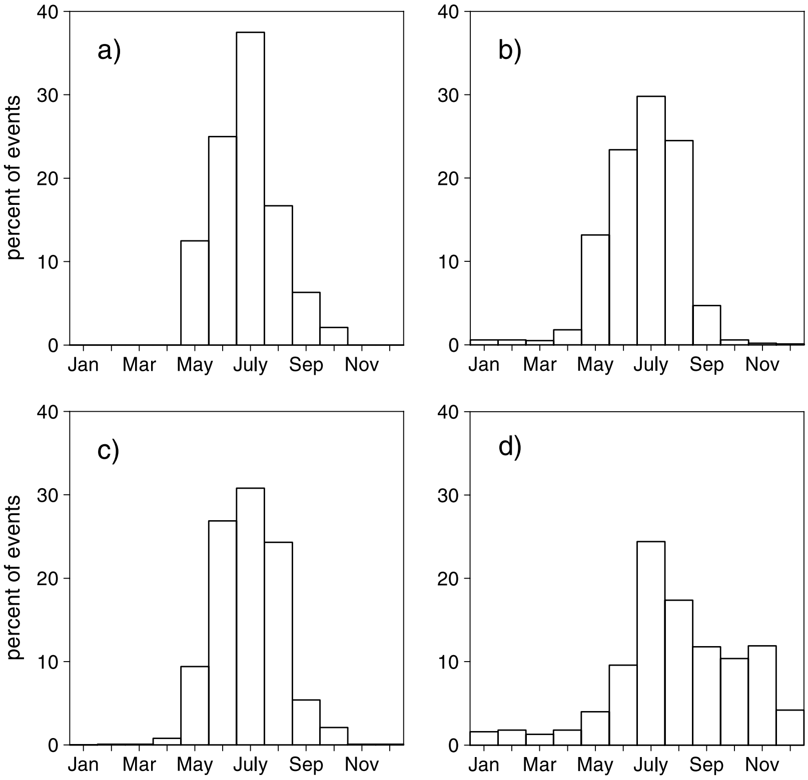

Figure 2. Seasonality of extreme storms [from *Gutknecht and Watzinger*, 1996]: Number of extreme storms (expressed in percentages) versus month for four example regions in Austria, (a) Moldau, (b) Donau between Enns and March, (c) Raab, and (d) Drau. "Extreme storms" are defined as those storms that have the property that $d > \sqrt{5t_r}$, where t_r is rainfall duration in minutes and d is the total rainfall depth in millimeters. Histograms in Figures 2a–2d are based on 48, 1795, 1512, and 3071 storms, respectively.

standard deviations between years and within each month of the runoff coefficients so defined. Both of these numbers show strong seasonal variation, and being measures of the antecedent condition of the catchment, they are likely to differently impact on the magnitude of the flood peaks that might result from storms that occur in different times of the year. The most dramatic effect is in Rattendorf (solid lines), where the runoff coefficient shows a bimodality that is in phase with, and therefore reinforces, the seasonality of extreme storms, thus contributing to the strong bimodality in the seasonal variation of annual maximum floods. The spring peak of the runoff coefficient appears to be associated with snowmelt while the autumn peak appears to be associated with heavy rainfall. In Teufelmühle (dashed lines) the apparent shift of the annual maximum flood peaks toward winter must be due to the high runoff coefficients obtained during the winter months, and not necessarily related to extreme storms. The high runoff coefficients in winter are a result of low evaporation and the presence of shallow snowpacks as indicated by the runoff simulations. *Merz et al.* [2004] have shown that the main effect of snowmelt on flood response in this type of catchments is in increasing antecedent soil moisture and hence runoff coefficients rather than through snowmelt contributions during the event. Wienerbruck is located at higher altitudes than Teufelmühle, so most of the snowmelt occurs in spring rather than in winter. The runoff coefficients in Figure 3b (dotted line) indeed peak in spring. The relatively flat response in Anger (dashed dotted lines) appears to be related to the rather flat variation of runoff coefficient and base flow during the year, and this suggests that the distribution of extreme storms is therefore the dominant control.

[11] Our basic hypothesis in this paper therefore is that the interactions between seasonality of rainfall characteristics and the seasonality of antecedent conditions can lead to the complex patterns of flood frequency behavior shown in Figure 1. We further hypothesize that these interactions can also be reflected in interesting regional/spatial patterns of flood frequency behavior. By way of illustration of the latter phenomenon, we present in Figure 4 regional patterns of flood frequency behavior for Austria [*Merz et al.*, 1999]. Figure 4a presents the timing of all of the recorded annual maximum floods over a period of about 40 years regardless of return period, and presented as a map of arrows. On the other hand, Figure 4b presents the seasonality of only the three largest recorded floods (high return periods). The length of the arrows is a measure of the strength of the seasonality: r = 1 if the floods occur on the same day of the year; r = 0 if the floods occur uniformly around the year. The direction of each arrow gives the mean timing of the floods in terms of day of the year counted from 1 January. Very low seasonalities are indicated as disks. The arrows in Figure 4b are significantly longer than those in Figure 4a, which indicates a narrowing

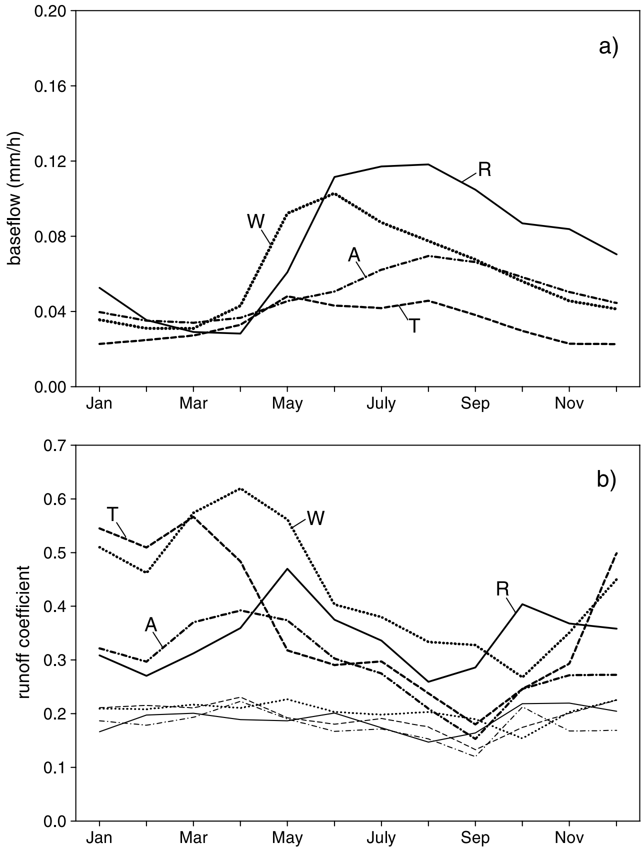

Figure 3. Seasonal base flow and runoff coefficient for four example catchments in Austria: Teufelmühle (dashed lines), Wienerbruck (dotted lines), Anger (dash-dotted lines), and Rattendorf (solid lines). (a) Base flow (minimum of daily runoff in each month, averaged over 30 years). (b) Runoff coefficient estimated by a rainfall-runoff model, averaged over each month and averaged over 30 years (thick lines) and standard deviation between years and within month of the runoff coefficient (thin lines).

down in the timing of annual maximum floods with increasing return period similar to what we saw in Figure 1 for a few of the catchments. However, the observed timings of the largest floods also display strong regional variations, suggesting that the interactions between extreme storms and antecedent conditions are highly spatially heterogeneous, being dependent on the heterogeneity of the climatic and catchment characteristics governing the generation of floods. Figure 4 suggests that the flood processes may indeed change as one moves from moderate to extreme floods.

[12] A major objective of this paper therefore is to explore the connection between the seasonality of floods and the climatic and catchment properties that govern the generation of these floods. However, while we are motivated by these empirical observations, the objective of the paper is limited to presenting a quasi-analytical framework within which to investigate these interactions. At this time, we are not endeavoring to recreate, through a modeling exercise, the exact temporal patterns presented for the four individual catchments (Figure 1), nor the observed regional patterns (Figure 4). From this perspective the work presented here represents the initial steps of a much more long-term investigation.

3. Quasi-analytical Derived Flood Frequency Model

[13] The approach proposed here is a generalization of the derived flood frequency approach presented by *Eagleson* [1972] and subsequently adapted and extended by others [e.g., *Sivapalan et al.*, 1990; *Fiorentino and Iacobellis*, 2001]. We will use the derived flood frequency approach to construct "monthly" flood frequency curves, for each month of the year, which we will then combine into "annual" flood frequency curves based on the "theory of mixed distributions" [*Buishand and Demaré*, 1990].

3.1. Details of the Stochastic Rainfall Model

[14] The stochastic rainfall model used here is an adaptation of the one used previously by *Robinson and Sivapalan* [1997a]. The model is adapted for conditions in Austria, and the parameters of the model are adjusted to mimic the observed rainfall record at Frankenfels station in the east of the country. The essential details of the model are presented next for completeness, with the parameter values adopted summarized in Table 1. Essentially, the model consists of discrete rainfall events whose arrival times, durations, average rainfall intensity and the within-storm intensity patterns are all random, governed by specified distributions. In addition, the parameters of these distributions are assumed to be seasonally dependent. At this stage, we have ignored spatial variability of the rainfall intensities.

3.1.1. Storm Duration and Interstorm Period

[15] Guided by data, storm duration, t_r, and interstorm period, t_b, are assumed to follow the Weibull distribution (probability density function or pdf), with parameters that vary seasonally, i.e.,

$$f_{T_r}(t_r|\gamma_r) = \frac{\beta_r}{\gamma_r}\left(\frac{t_r}{\gamma_r}\right)^{\beta_r-1}\exp\left(-\frac{t_r}{\gamma_r}\right)^{\beta_r} \qquad t_r > 0 \qquad (1a)$$

$$\gamma_r = \mu_r\left(\Gamma\left(1+\frac{1}{\beta_r}\right)\right)^{-1} \qquad (1b)$$

$$f_{T_b}(t_b|\gamma_b) = \frac{\beta_b}{\gamma_b}\left(\frac{t_b}{\gamma_b}\right)^{\beta_b-1}\exp\left(-\frac{t_b}{\gamma_b}\right)^{\beta_b} \qquad t_b > 0 \qquad (2a)$$

$$\gamma_b = \mu_b\left(\Gamma\left(1+\frac{1}{\beta_b}\right)\right)^{-1} \qquad (2b)$$

where β_r and β_b are the shape parameters of the Weibull distributions, and γ_r and γ_b are the scale parameters which can be expressed by the mean storm duration μ_r, and the mean interstorm period μ_b. These are allowed to vary sinusoidally with time of year, τ, as follows:

$$\mu_r = \delta_r + \alpha_r\cos\left\{\frac{2\pi}{\omega}(\tau-\tau_r)\right\} \qquad (3)$$

$$\mu_b = \delta_b + \alpha_b\cos\left\{\frac{2\pi}{\omega}(\tau-\tau_b)\right\} \qquad (4)$$

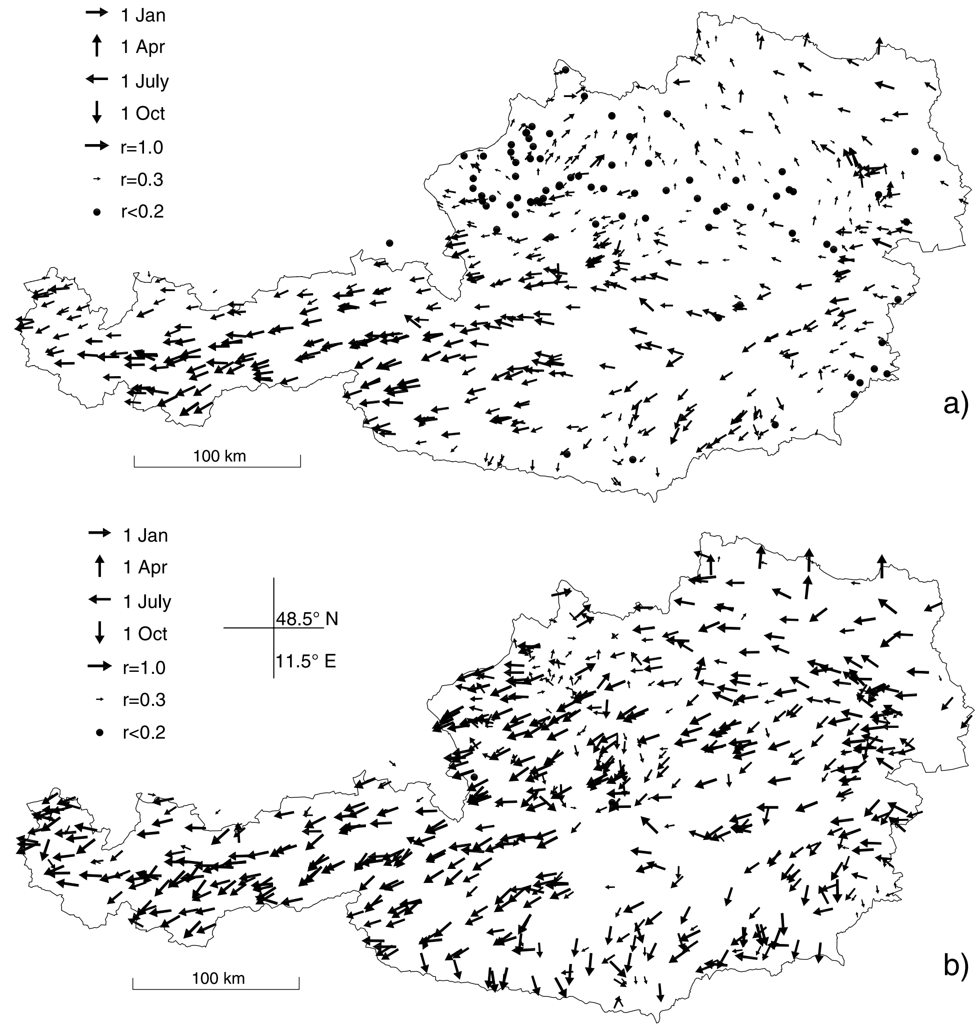

Figure 4. Flood seasonality in Austria [from *Merz et al.*, 1999]. The direction of the arrows indicates the average occurrence of floods in a year, and the length of the arrows is a measure of the strength of the seasonality. (a) All maximum annual floods. (b) Only the three biggest floods on record.

where δ_r and δ_b are annual average storm duration and interstorm period, respectively, τ_r and τ_b are seasonal phase shifts, α_r and α_b are the amplitudes of the seasonal variations of t_r and t_b, τ describes the time of year, and ω is the total number of time units in a year (i.e., $\omega = 12$ months if τ, τ_r and τ_b are in month units). α_r α_b, δ_r, δ_b, τ_r and τ_b have simply been estimated by fitting equations (3) and (4) to seasonal plots of mean storm duration and mean interstorm period derived from the Frankenfels rainfall time series. β_r and β_b were assumed to be constant throughout the year and were estimated from the distribution of storm duration and interstorm period of the rainfall data. The data also indicated that the observed distributions can be closely approximated by Weibull distributions.

3.1.2. Rainfall Intensities

[16] We describe the mean storm rainfall intensity i as a random variable stochastically dependent upon storm duration, t_r, i.e., i and t_r follow the joint pdf, $f_{I,T_r}(i, t_r)$, which is also seasonally varying due to the variation of γ_r with time of year, τ. The mean storm rainfall intensity is disaggregated further to hourly intensity patterns using stochastically generated mass curves [*Huff*, 1967], as shown later.

3.1.3. Average Storm Rainfall Intensity

[17] To parameterize the dependence between i and t_r we assumed the conditional statistics of $E[i|t_r]$ and CV^2 $[i|t_r]$ to be power functions of t_r as follows:

$$E[i|t_r] = a_1 t_r^{b_1} \qquad \text{and} \qquad CV^2[i|t_r] = a_2 t_r^{b_2} \tag{5}$$

with the coefficient a_1 being assumed to also vary seasonally, as follows, to account for variability of rainfall generating mechanisms within the year:

$$a_1 = \delta_a + \alpha_a \cos\left\{\frac{2\pi}{\omega}(\tau - \tau_a)\right\} \tag{6}$$

The power functions given in equation (5) provide relationships between t_r and the first two moments of f_I $(i|t_r)$, the conditional distribution of i given t_r, which is assumed to follow the gamma distribution:

$$f_I(i|t_r) = \frac{\lambda}{\Gamma(\kappa)}(\lambda i)^{\kappa-1}\exp(-\lambda i) \tag{7}$$

Table 1. Parameters of the Rainfall and Runoff Models

Parameter	Symbol	Equation	Value Used in Figure 8	Value Used in Figure 9	Value Used in Figure 10	Value Used in Figures 11a and 12a	Value Used in Figures 11b and 12b	Units
Weibull parameter of storm duration	β_r	(1)	0.7	0.7	0.7	0.7	0.7	
Weibull parameter of inter-storm period	β_b	(2)	0.7	0.7	0.7	0.7	0.7	
Annual average storm duration	δ_r	(3)	5.7	5.7	5.7	5.7	5.7	hours
Amplitudes of the seasonal variation of storm duration	α_r	(3)	1.4	1.4	1.4; 0	1.4	1.4	hours
Month of maximum storm duration	τ_r	(3)	0	0	0	0	0	months
Annual average interstorm period	δ_b	(4)	43.0	43.0	43.0	43.0	43.0	hours
Amplitudes of the seasonal variation of interstorm period	α_b	(4)	5.6	5.6	5.6; 0	5.6	5.6	hours
Month of maximum interstorm period	τ_b	(4)	0	0	0	0	0	months
Rainfall model parameter	a_2	(5)	1.5	1.5	1.5	1.5	1.5	
Rainfall model parameter	b_1	(5)	0.01	0.01	0.01	0.01	0.01	
Rainfall model parameter	b_2	(5)	−0.55	−0.55	−0.55	−0.55	−0.55	
Parameter of mean rainfall intensity	δ_a	(6)	1.05	1.05	1.05	1.05	1.05	mm h^{-b_1-1}
Amplitude of rainfall intensity	α_a	(6)	0.65	0.65	0.65	0.65	0.65	mm h^{-b_1-1}
Month of maximum rainfall intensity	τ_a	(6)	6	6	6	6	6	months
Annual average base flow	δ_q	(9)	0.065	0.065	0	0	0	mm/h
Amplitude of the seasonal variation of base flow	α_q	(9)	0.035	0.035	0	0	0	mm/h
Month of maximum base flow	τ_q	(9)	6.5	6.5	-	6.5	6.5	months
Annual average runoff coefficient	δ_c	(10)	0.35	0.35	0.35	0.35	0.35	
Amplitude of the seasonal variations of the runoff coefficient	α_c	(10)	0.25	0.25	0.25; 0	0.25	0.25	
Month of maximum runoff coefficients	τ_c	(10)	3.5	3.5	variable	6	3	months
Variance of the random component of the runoff coefficient	σ_c^2	(12)	0	0; 0.04	0.04	0.04	0.04	
Catchment response time for flood events	t_c	(13), (14)	6.0	6.0	6.0	6.0	6.0	hours
Mean of the rescaled χ ratio of flood peaks	μ_η	(16)	-	0.3	0.3	0.3	0.3	
Variance of the rescaled χ ratio of flood peaks	σ_η^2	(16)	-	0.04	0.04	0.04	0.04	

with the gamma parameters, κ and λ being functions of t_r. By matching expressions for the statistics of the general gamma distribution with equation (5), we can estimate κ and λ as follows:

$$\kappa = \frac{t_r^{-b_2}}{a_2} \text{ and } \lambda = \frac{t_r^{-b_1-b_2}}{a_1 a_2} \tag{8}$$

The parameters b_1, b_2, a_2, δ_a, α_a and τ_a have been estimated by fitting equations (5) and (6) to the rainfall data at Frankenfels.

3.2. Details of the Simple Rainfall-Runoff Model

[18] The rainfall-runoff model used in the study is rather simple, as the main motivation is to present the generalized derived flood frequency framework, and validate it using results from the Monte Carlo approach. The rainfall-runoff model consists of three components: (1) a base flow component, which is assumed to be seasonally varying; (2) a quick flow component that utilizes a single runoff coefficient, whose variation within the year has a seasonal component (i.e., its mean) and a random component (i.e., deviation from the mean); and (3) a runoff routing component which consists of a linear reservoir with a response time of t_c. The details of these three components are given below.

[19] 1. The first component is initial flow in the river (base flow). Base flow q_0 is assumed to vary seasonally according to the sinusoidal expression

$$q_0 = \delta_q + \alpha_q \cos\left\{\frac{2\pi}{\omega}(\tau - \tau_q)\right\} \tag{9}$$

No randomness is allowed in the case of the base flow variation.

[20] 2. The second component is quick flow runoff generation and the runoff coefficient. The volume of runoff generation during a storm is estimated according to a specified runoff coefficient, r_c, (fixed for the event and thus nonlinearity is not considered), the mean of which is assumed to vary seasonally, i.e., with the time of occurrence of the storm, as follows:

$$r_{cm} = \delta_c + \alpha_c \cos\left\{\frac{2\pi}{\omega}(\tau - \tau_c)\right\} \tag{10}$$

In addition to the seasonal variation, the runoff coefficient is also assumed to contain a random element. For simplicity, and on the basis of empirical results (see Figure 3), we assume that the variance of the random component remains constant throughout the year at a value equal to σ_c^2. We assume further based on previous work of *Gottschalk and Weingartner* [1998] that r_c is distributed according to the beta distribution:

$$f_R(r_c) = \frac{1}{B(u,v)} r_c^{u-1}(1 - r_c)^{v-1} \quad 0 < r_c < 1,\ u > 0, v > 0 \tag{11}$$

where $B(u, v)$ is the incomplete beta function, and given the mean and standard deviation of runoff coefficient as above,

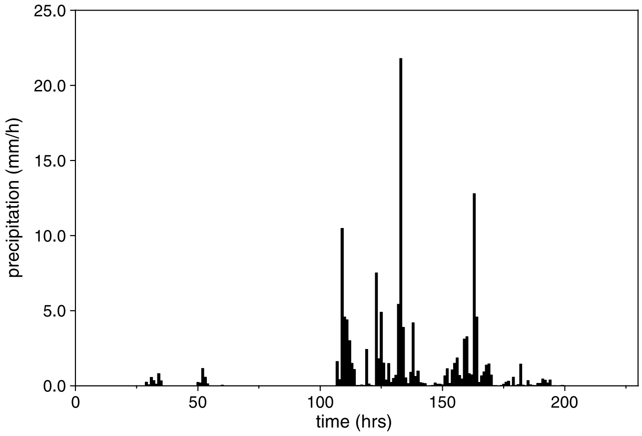

Figure 5. Typical simulated hyetograph (a major event in October).

the parameters u and v of the beta distribution can then be estimated from:

$$u = \frac{r_{cm}^2(1 - r_{cm})}{\sigma_c^2} - r_{cm} \tag{12a}$$

$$v = \frac{r_{cm}(1 - r_{cm})^2}{\sigma_c^2} - (1 - r_{cm}) \tag{12b}$$

In the model the runoff coefficients represent the lumped effect of a number of processes that vary seasonally including evaporation and snowmelt as well as random processes such as antecedent rainfall.

[21] 3. The final component is runoff routing. For routing purposes, we conceptualize the catchment as a linear reservoir with a response time t_c. Effectively, this is equivalent to the convolution of the time series of quick flow generation with an exponential instantaneous unit hydrograph (IUH). For a single storm, the transformation of rainfall to runoff can be expressed through the convolution integral given below:

$$q(t) = q_0 + \frac{r_c}{t_c}\int_0^t i(t)\exp\left(-\frac{t - t'}{t_c}\right)dt' \tag{13}$$

where $i(t)$ is the rainfall input time series, and $q(t)$ is the resulting runoff time series. For response time t_c, we used a typical value of medium sized catchments in Austria of 6 hours.

3.3. Effect of Within-Storm Patterns on Flood Peaks

[22] In this paper we are interested in the flood peak resulting from the above convolution for all the storms occurring in the year. For the Monte Carlo simulation approach (to be presented later), this is fairly straightforward, and only involves repeated application of equation (13) for the entire rainfall record.

[23] For the quasi-analytical approach, however, we require analytical or quasi-analytical expressions for the flood peak in terms of the average rainfall intensity, duration, also accounting for within-storm patterns. This is not so straightforward, and in this section we present an approximate approach that involves the implementation of a random correction factor χ to account for the random nature of within-storm patterns.

[24] To illustrate this, consider a single storm of average intensity, i, and of duration, t_r. For a constant storm runoff coefficient, r_c, the depth of (new) runoff generated is $r_c \cdot i \cdot t_r$. As a base case, let us assume that the rainfall intensity within the storm is also constant. Under these simplifying assumptions, by completing the integration in equation (13) we can easily derive an expression for the flood peak as follows:

$$q_p = q_0 + r_c \cdot i \cdot \chi \cdot \left(1 - \exp\left(-\frac{t_r}{t_c}\right)\right) \tag{14}$$

where for the simple rainfall pattern used in this base case, a correction factor is indeed not needed, and $\chi = 1$. To come up with a priori estimates for χ for more complex within-storm patterns, we utilized synthetic time series of rainfall intensities, generated using the rainfall model presented earlier, with variable duration, average intensity but including within-storm temporal patterns. The within-storm temporal patterns are generated using *Robinson and Sivapalan*'s [1997a] cascade method which is summarized in Appendix A. An example of a typical storm is presented in Figure 5 which, by visual inspection, is similar to observed storm patterns. As a check of the ability of the rainfall model to reproduce observed patterns of variability in the observed record at Frankenfels, we carried out a number of comparisons. As an example, cumulative mass curves are shown in Figure 6, including the mean and the 0.1 and 0.9 quantiles all of which mimic the corresponding patterns in the observed record. The cascade model in Appendix A is used to find values for χ and it is also used in the Monte Carlo approach discussed later but it is not directly used in the quasi-analytical derived flood frequency model.

[25] For finding values for χ, each of the storms so produced is routed through a linear store, as in equation

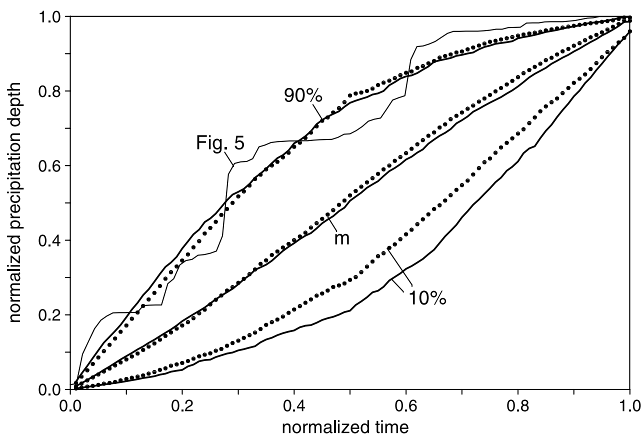

Figure 6. Mass curves (see equation (A1)). Thick lines are the 10 and 90% quantiles and mean of simulations. Dots are the 10 and 90% quantiles and mean from 7 years of hourly rainfall data at the Frankenfels rain gauge. Thin line is the mass curve of the simulated event in Figure 5.

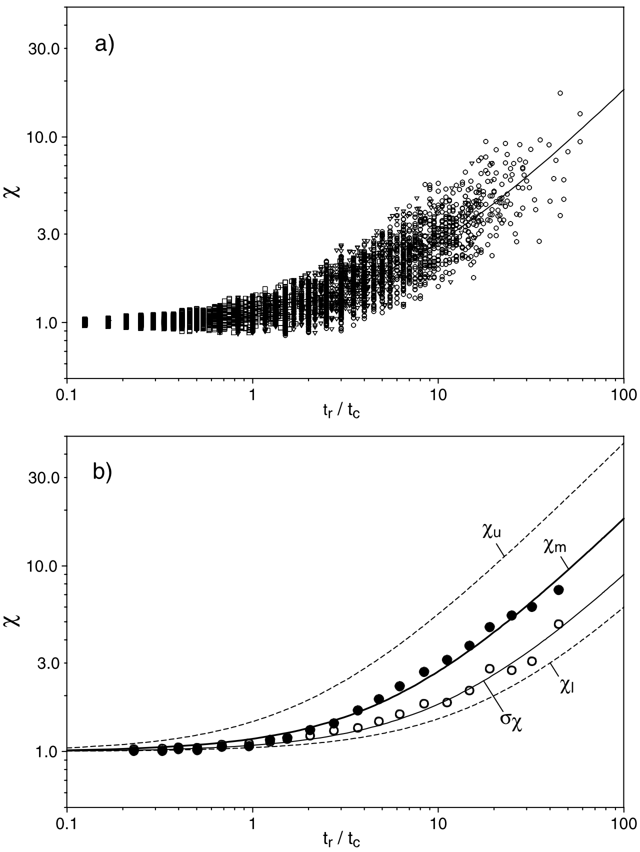

Figure 7. Effect of time patterns (i.e., within storm temporal rainfall patterns) on peak flow, as expressed in terms of the χ ratio. Here t_r is the storm duration, and t_c is the catchment response time. (a) χ from Monte Carlo simulations (circles, t_c = 2 hours; triangles, t_c = 6 hours; squares, t_c = 24 hours) with fitted mean χ indicated as a solid line. (b) Fitted upper and lower envelopes (dashed lines), mean from Monte Carlo simulations for a number of t_r/t_c classes (solid circles), fitted mean (thick solid line); 1 + standard deviation from Monte Carlo simulations (open circles), and 1 + fitted standard deviation (thin solid line).

(13), for three different specified response times t_c. For each t_c this kind of filtering produces a synthetic runoff record for each storm, which is analyzed to identify the single flood peak for each storm. Clearly, the required correction factor χ for estimation of the flood peak using equation (14) is a number generally greater than 1, and also random due to the random nature of the within-storm patterns. We also find that, on average, increasing t_c leads to a reduction of the magnitude of the flood peak, and thus χ.

[26] In order to obtain a simple expression for χ we plotted it against t_r/t_c, the ratio of storm duration to response time, and as shown in Figure 7a, we find that it collapses into a single scatterplot regardless of the individual values of t_r and t_c used. However, there is considerable scatter about the mean curve, arising from the randomness of the within-storm patterns. To account for the scatter we fitted four curves: the lower and upper envelopes (χ_l and χ_u) of the scatterplots, and the mean and standard deviation (χ_m and $\sigma\chi$) for each value of t_r/t_c. Figure 7b presents the fitted curves, which are expressed analytically as follows:

$$\chi_m = 1 + \chi_m' \frac{t_r}{t_c} \tag{15a}$$

$$\sigma_\chi = \sigma_\chi' \frac{t_r}{t_c} \tag{15b}$$

$$\chi_l = 1 + \chi_l' \frac{t_r}{t_c} \tag{15c}$$

$$\chi_u = 1 + \chi_u' \frac{t_r}{t_c} \tag{15d}$$

where $\chi_m' = 0.17$, $\sigma_\chi' = 0.08$, $\chi_l' = 0.05$, $\chi_u' = 0.45$. These parameters are a function of the models chosen for rainfall (i.e., within storm patterns) and the runoff response, but are independent of the actual event characteristics used in their estimation, namely t_r and t_c. Let us consider a new random variable η, which is a scaled version of the χ ratio defined above, with the property that $0 \leq \eta \leq 1$, as follows:

$$\eta = \frac{\chi - \chi_l}{\chi_u - \chi_l} \tag{16a}$$

or

$$\chi = \chi\left(\frac{t_r}{t_c}, \eta\right) = \chi_l + \eta\{\chi_u - \chi_l\} \tag{16b}$$

The mean, μ_η, and variance, σ_η^2, of the rescaled ratio of flood peaks, η, can then be estimated using the expressions given in equations (15a) to (15d). Upon doing this, remarkably, we find that the mean and variance collapse to being mere constants, and completely independent of t_r/t_c, that is,

$$\mu_\eta = \frac{\chi_m - \chi_l}{\chi_u - \chi_l} = \frac{\chi_m' - \chi_l'}{\chi_u' - \chi_l'} \tag{17a}$$

$$\sigma_\eta^2 = \frac{\sigma_\chi^2}{(\chi_u - \chi_l)^2} = \frac{\sigma_\chi'^2}{(\chi_u' - \chi_l')^2} \tag{17b}$$

[27] This is a highly convenient result, yielding $\mu_\eta = 0.3$ and $\sigma_\eta^2 = 0.04$. We further assume that η is also distributed according to the beta distribution:

$$f_H(\eta) = \frac{1}{B(\rho, \vartheta)} \eta^{\rho-1}(1-\eta)^{\vartheta-1} \qquad 0 < \eta < 1, \rho > 0, \vartheta > 0 \tag{18}$$

where $B(\rho, \vartheta)$ is the incomplete beta function. As in the case of the runoff coefficient, the parameters ρ and ϑ are then given by

$$\rho = \frac{\mu_\eta^2\left(1-\mu_\eta\right)}{\sigma_\eta^2} - \mu_\eta \tag{19a}$$

$$\vartheta = \frac{\mu_\eta\left(1-\mu_\eta\right)^2}{\sigma_\eta^2} - \left(1-\mu_\eta\right) \tag{19b}$$

Note that the properties of the χ and η ratios presented above, i.e., μ_η = 0.3 and σ_η^2 = 0.04, are a function of the nature of the within-storm patterns, i.e., the cascade model used to generate these within-storm patterns, and the rainfall-runoff model used for the runoff generation and routing. More complex models of both rainfall and runoff routing may lead to different properties of the χ ratio. For example, nonlinearity of the rainfall-runoff process will lead to higher χ ratios. More detailed investigation of the interactions of the rainfall model and the rainfall-runoff model can lead to significant improvements in the accuracy of flood estimates, and is left for further research.

3.4. Quasi-analytical Derived Flood Frequency Framework

3.4.1. Probability Distribution of the Population of Flood Peaks

[28] Flood frequency analysis concerns the estimation of annual peak discharges with specified probabilities of exceedance. If we let a random variable Y denote the peak discharge of all independent storms, and Q denote the annual maximum peak discharge, then the probability distribution of Q is the extreme value distribution associated with Y. Noting that the rainfall inputs i and t_r are random variables (potentially also dependent on each other), we can derive the probability distribution of Y in terms of the probability density functions of i and t_r, using derived distribution theory [*Eagleson*, 1972; *Wood*, 1976; *Robinson and Sivapalan*, 1997b]. Given the joint probability density function of i and t_r as $f_{I,T_r}(i, t_r)$, the cumulative distribution of Y is given by:

$$F_Y\left(q_p\right) = \Pr\left[Y \le q_p\right] = \iint_R f_{I,T_r}(i,t_r)di\ dt_r \tag{20}$$

Here $F_Y(q_p)$ is the probability, for a given flood event, that the flood peak Y is less than or equal to q_p. For the rainfall-runoff model given by equation (14), R is the region such that $q_p \geq q_0 + r_c\, i\chi[1 - \exp(-t_r/t_c)]$. Then, using equation (20) for the simplifying case where χ and r_c are allowed to remain constant for all storms, the above integral simplifies to

$$F_Y\left(q_p\right) = \int_0^\infty F_I\left\{\frac{q_p - q_0}{r_c \cdot \chi[1-\exp(-t_r/t_c)]}|t_r\right\} f_{T_r}(t_r)dt_r \tag{21}$$

where $F_I(.|t_r)$ is the conditional cumulative distribution of rainfall intensity, conditioned on t_r.

3.4.2. Conversion to Extreme Value Distribution

[29] Assuming m independent floods in a year, the extreme value distribution is formed by selecting the largest of these m floods in each year, and deriving the distribution function of the truncated series. Using the theory of order statistics [*Mood et al.*, 1974; *Kottegoda and Rosso*, 1997], the cdf of annual maximum floods, denoted by $F_Q(q_p)$, is given by

$$\Pr\left[Q > q_p\right] = 1 - F_Q\left(q_p\right) = 1 - \left[F_Y\left(q_p\right)\right]^m \tag{22}$$

The same result can also be expressed in terms of a return period (in years):

$$T = \left\{\Pr\left[Q > q_p\right]\right\}^{-1} = \left\{1 - F_Q\left(q_p\right)\right\}^{-1} = \left\{1 - \left[F_Y\left(q_p\right)\right]^m\right\}^{-1} \tag{23}$$

3.4.3. Seasonal Variability of Climate and Antecedent Conditions

[30] The above result is only valid if the rainfall and catchment properties do not vary systematically within the year. The effects of seasonal variability, if present, must somehow be factored in the derivation. Let us suppose that pdfs of i and t_r vary seasonally, as do the runoff coefficient, r_c, and initial base flow, q_0. We will assume that these pdfs remain sufficiently stationary within individual months, so that the integral in equation (21) can still be carried out in the normal way for each month. For simplicity we will here assume that the χ ratio for rainfall temporal variability remains constant for all months. Thus, for any month j, j = 1,...12, we can rewrite the integral of equation (21) as follows:

$$F_Y^j\left(q_p\right) = \int_0^\infty F_I^j\left\{\frac{q_p - q_0^j}{r_c^j\chi[1-\exp(-t_r/t_c)]}|t_r\right\} f_{T_r}^j(t_r)dt_r \tag{24}$$

[31] At this point we generalize the above result by introducing random variability of both runoff coefficient and the χ ratio. Using the probability density functions derived before for runoff coefficient and the scaled ratio of flood peaks, η, we then have

$$F_Y^j\left(q_p\right) = \int_0^1\int_0^1\int_0^\infty F_I^j\left\{\frac{q_p - q_0^j}{r_c^j[\chi_l + \eta(\chi_u - \chi_l)]\cdot[1-\exp(-t_r/t_c)]}|t_r\right\} \cdot f_T^j(t_r) f_R^j(r_c) f_H(\eta) dt_r dr d\eta \tag{25}$$

where it should be noted that χ_u and χ_l are empirical functions of t_r/t_c.

[32] Let us assume that the number of flood peaks in month j, is m_j, j = 1, ... 12. Then, equation (23) can be rewritten for each month of the year, as follows:

$$T = \left\{1 - \left[F_Y^j\left(q_p\right)\right]^{m_j}\right\}^{-1} \tag{26}$$

[33] We will term the resulting flood frequencies monthly flood frequency curves, since they relate to probability of

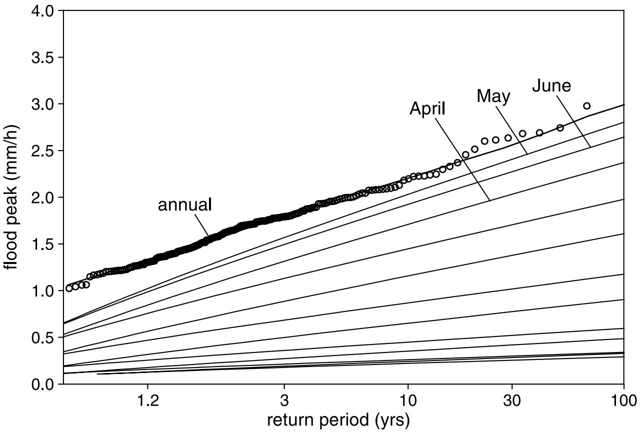

Figure 8. Monthly (thin lines) and annual (thick line) quasi-analytical derived flood frequency curves and annual flood frequency curves from Monte Carlo simulations (circles). No time patterns are used, and runoff coefficient is seasonal but not random. Horizontal scale is linear using Gumbel reduced variates. For parameters, see Table 1.

exceedances of the given flood peak q_p within a single month, yet the return periods are in years, e.g., probability that the January flood peak exceeds q_p in any given year. Provided seasonal variations of all controlling variables are known, it is straightforward to compute, using equations (25) and (26), the monthly flood frequency distributions for all 12 months.

3.4.4. Derivation of Annual Flood Frequency and Mixed Distributions

[34] For many engineering applications, we want to derive the annual flood frequency, i.e., the probability that the annual flood peak (maximum of the 12 monthly maxima) exceeds a given q, and the corresponding return period. Here this will be accomplished using the theory of mixed distributions, noting that the cdfs of the flood peaks for each month are different and the cdf of annual maxima is thus drawn from a mixture of these. Assuming the flood peaks in month j are independent from those in month $j + 1$ and considering the number of flood peaks in month j, m_j, $j = 1, \ldots 12$, again using order statistics [*Mood et al.*, 1974; *Kottegoda and Rosso*, 1997; *Buishand and Demaré*, 1990], we can show that

$$\Pr[Q > q_p] = 1 - F_Q(q_p) = 1 - \prod_{j=1}^{12} \left[F_Y^j(q_p)\right]^{m_j} \tag{27}$$

$$T = \{\Pr[Q > q_p]\}^{-1} = \left\{1 - \prod_{j=1}^{12} \left[F_Y^j(q_p)\right]^{m_j}\right\}^{-1} \tag{28}$$

[35] Note above that, essentially, mixing of the monthly flood frequency curves is equivalent to estimating the product of the monthly nonexceedance probabilities, under the product sign in equations (27) and (28). It can be shown to be invariant of the number of stationary periods used (i.e., in this case a month), provided that the number of events in a year are preserved. Equations (22) and (27) are based on the assumption of the independence of individual events. While this assumption is clearly appropriate for the annual case (equation (22)) it is less obviously so for the monthly case (equation (27)) and will be checked by Monte Carlo simulations.

4. Monte Carlo Simulation Approach

[36] The continuous or Monte Carlo simulation approach is used to check the integration and the χ ratio approximation adopted by the quasi-analytical derived flood frequency approach as well as the assumption of independence of monthly flood peaks. The steps involved in the Monte Carlo approach are summarized as follows.

[37] 1. Synthetically generate (where necessary multiple realizations of) continuous time series of rainfall intensities, using the rainfall model presented in section 3.1 and in Appendix A, using parameters presented in Table 1.

[38] 2. Apply the runoff coefficient, for each storm, incorporating the seasonality and randomness on a storm by storm basis as per the date that the storm occurred, multiply the rainfall time series by this runoff coefficient.

[39] 3. Convolute the resulting runoff generation time series with the exponential IUH presented in equation (13) with response time t_c being assumed to remain constant with date, and add the seasonally varying base flow at the end.

[40] 4. Scan the resulting continuous time series and pick the largest flood in each month (forming the monthly maxima data series), and in the whole year (annual maxima data series), and construct the monthly and annual flood frequency curves.

5. Results

5.1. Test of the Generalized Derived Flood Frequency Approach

[41] As a test of the derived flood frequency approach we compare the estimated flood frequency curve for the case with no within-storm patterns, against the corresponding predictions by the Monte Carlo method. For both the rainfall and the catchment models, parameters that are typical of Austrian conditions have been used (Table 1). For this application, the runoff coefficient is assumed to vary seasonally, but no randomness is included. The results are presented in Figure 8. All flood peaks are expressed in terms of runoff depths (mm/h). Given the catchment response time of 6 hours assumed here, the average hourly values (Monte Carlo simulations) are comparable with the instantaneous values of the quasi-analytical approach. The 1 mm/h of runoff depth is equivalent to a specific peak discharge of 0.28 $m^3/s/km^2$. The annual flood frequency curve resulting from the quasi-analytical approach (thick solid line in Figure 8) is close to that resulting from the Monte Carlo approach (circles) suggesting that the generalized derived flood frequency approach presented in this paper captures the seasonality and that the integration is correct. Figure 8 also presents the monthly flood frequency curves (thin lines). The probability that a given flood peak discharge occurs in a particular month is smaller (larger T) than for it to occur at any time of the year. The monthly flood frequency curves hence plot to the right of the annual curve in Figure 8. For a flood peak of, say, 1.5 mm/h the annual return period is 1.4 (equivalent to a nonexceedance

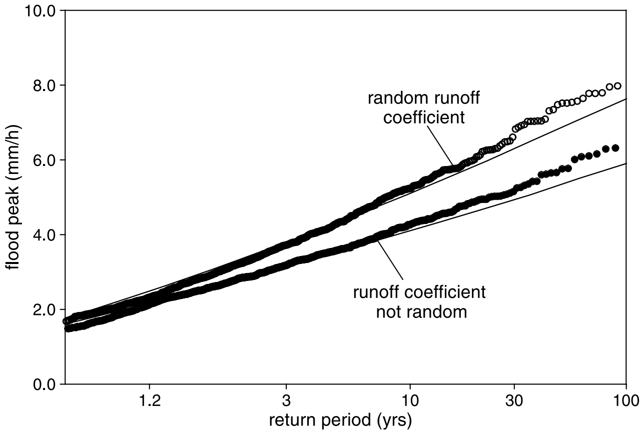

Figure 9. Annual flood frequency curves using time patterns from the quasi-analytical (lines) and Monte Carlo (dots) methods. Bottom line shows the case with within-storm time patterns included, runoff coefficient seasonal but not random. Top line shows the case with storm time patterns included, runoff coefficient seasonal and random.

probability of 0.30) while the monthly return periods are 2.8, 3.0, 5.5 .... (equivalent to nonexceedance probabilities F_Y^j of 0.64, 0.67, 0.82 ...). The annual nonexceedance probability of 0.30 is simply the product of the monthly nonexceedance probabilities. The monthly flood frequency curves for the summer months plot at the top while those for the winter months plot at the bottom indicating that big floods in winter are very unlikely for the parameters chosen here (Table 1).

5.2. Effect of Randomness of Within-Storm Patterns and Runoff Coefficient

[42] Figure 9 presents the estimated flood frequency curves when within-storm patterns are included (by both the quasi-analytical and Monte Carlo approaches). In the bottom line of Figure 9, the runoff coefficient is assumed to vary seasonally in a deterministic manner (no randomness is included). For small to medium return periods the Monte Carlo results are close to the results from the quasi-analytical approach. This suggests that the approximate analytical χ ratio approach adequately captures the effects of within-storm temporal patterns on the flood peaks. However, for return periods larger than about 30 years, the quasi-analytical approach seems to slightly underestimate flood peaks and the flood frequency curve is slightly less curvilinear than in the case of the Monte Carlo simulations. This suggests that the χ ratio approximation is somewhat more linear than the explicit time patterns and the probability of extreme events is slightly underestimated.

[43] As compared to Figure 8, the bottom line in Figure 9 gives almost twice the flood peak for the same return period. This is the effect of within-storm temporal patterns. It is clear that the inclusion of rainfall time patterns is critically important for realistic derived flood frequency predictions.

[44] We also present in Figure 9 the results of the case where the runoff coefficient varies both seasonally (in the mean) along with a random component (top line in Figure 9). With the addition of the random component, the flood frequency curve not only increases on average (shifts upward), but it also increases in steepness. When allowing for random runoff coefficients a small number of events occur where large runoff coefficients (wet antecedent moisture conditions) coincide with large rainfall depths to produce very large flood peaks.

5.3. Further Insights into the Effects of Seasonality

[45] With the derived flood frequency model developed above, we next carry out additional simulations to gain further insights into the effects of seasonality. There are two ways that seasonality enters into the flood frequency curve: seasonality in the rainfall inputs, especially "extreme rainfalls," and the seasonality in the transformation between rainfall and runoff. The latter appears through the runoff coefficient and base flow in the present model, whose seasonality ultimately can be connected to seasonality of rainfall and evaporation. Figure 10 examines the effect of the interaction of these two types of seasonality on the flood frequency curve. Figure 10a shows the annual flood frequency curves for different phase shifts between seasonal

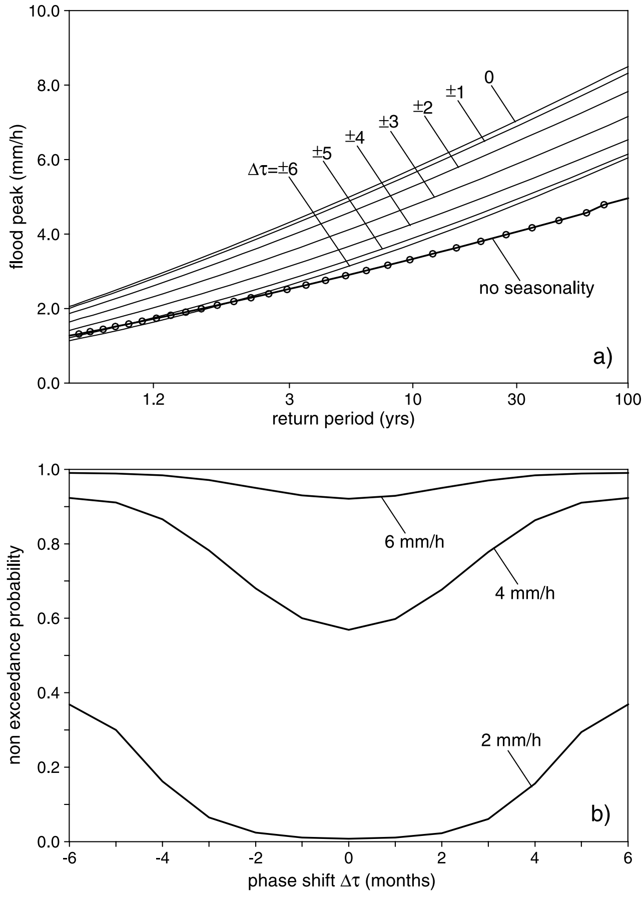

Figure 10. Effect of phase shift. (a) Annual flood frequency curves for different phase shifts $\Delta\tau$ of the runoff coefficient r_c as compared to rainfall ($\Delta\tau = \tau_c - \tau_a$ with $\tau_r = \tau_b = \tau_a - 6$; thin lines) and annual flood frequency curve without any seasonality (i.e., all amplitudes are 0; thick line with circles). (b) Nonexceedance probabilities F_Y^j for three flood peaks (2, 4, and 6 mm/h) as a function of phase shift $\Delta\tau$. A phase shift of $\Delta\tau = 0$ corresponds to highest runoff coefficients in the same month as the highest rainfall intensity.

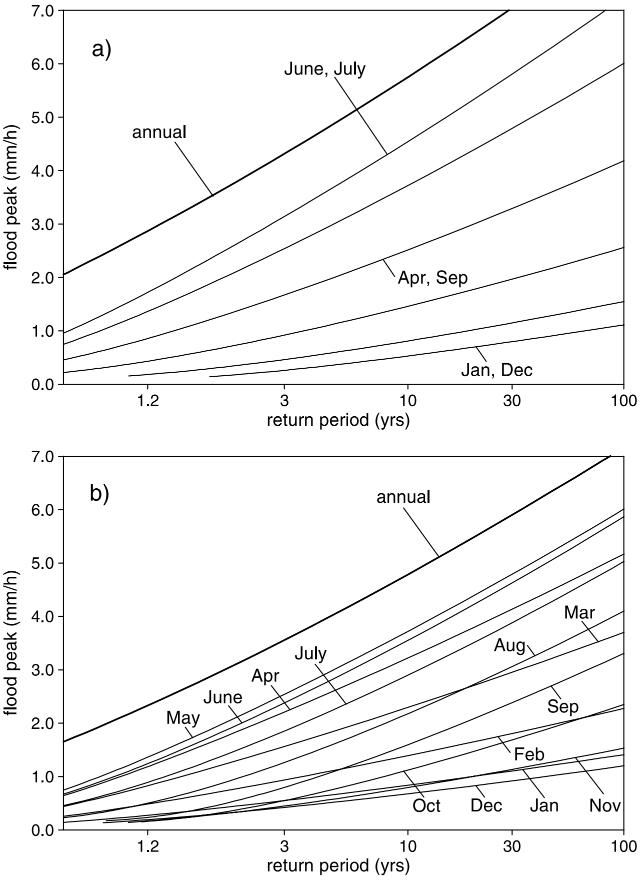

Figure 11. Flood frequency curves for different months (thin lines) and annual flood frequency curve (thick line). (a) Phase shift $\Delta\tau = 0$ (i.e., maximum rain in summer, maximum runoff coefficient r_c in summer). (b) Phase shift $\Delta\tau = -3$ months (i.e., maximum rain in summer, maximum r_c in spring).

variabilities of rainfall and runoff coefficient (thin lines). The phase shift is defined as $\Delta\tau = \tau_c - \tau_a$ with $\tau_r = \tau_b = \tau_a - 6$. Figure 10a also includes the base case with no seasonality either in the rainfall or in the runoff coefficient (thick line with circles). Figure 10a shows that the flood magnitude is largest when the rainfall and runoff coefficient are perfectly in phase, i.e., the phase shift $\Delta\tau = 0$, which means the highest runoff coefficients occur in the same month as highest rainfall intensity. This reflects a kind of resonance. The flood frequency curves decrease in magnitude when they become increasingly out of phase. It is interesting that any kind of seasonality (including out of phase) produces higher flood frequency curves than the case where no seasonality is included (thick line with circles in Figure 10). When seasonality is present a coincidence of large runoff coefficients (wet antecedent moisture conditions) with large rainfall depths is more likely than for the case without seasonality thus producing larger flood peaks. Note that the "resonance" highlighted above will be even more dramatic if the runoff generation process were to be nonlinear, with a runoff coefficient that increases with increased rainfall.

[46] Figure 10b presents the same results of Figure 10a in an alternative manner to illustrate the role of the nonexceedance probabilities. In this case, we estimate the nonexceedance probabilities for three different specified values of the flood peak (2, 4 and 6 mm/h). Essentially, this amounts to slicing Figure 10a horizontally at the three specified flood levels, reading off the return period for each phase shift, and then estimating the corresponding nonexceedance probabilities (=$1 - T^{-1}$). The results in Figure 10b show that the nonexceedance probability of a given flood peak is smallest for zero phase shift (case of resonance), and increases with increasing phase shift. For the largest of the flood peak values selected (6 mm/h) the exceedance probability varies from 0.01 (6 month phase shift) to 0.08 (no phase shift).

[47] Having determined the effect of seasonality of extreme storms and antecedent conditions on the magnitude of the annual and monthly flood frequency curves, we next investigate the question as to what are the relative contributions of individual months toward the annual flood frequency curve. In doing this we note at the outset that whereas in the observed record only one month produces the observed annual maximum flood in each year, the derived flood frequency approach can generate the relative contributions of the various months toward the annual maximum flood, i.e., the probability that the annual maximum flood of a given return period would occur in a specified month, although this cannot be verified in practice with the limited length of record currently available.

[48] Figure 11 presents the flood frequency curves for different months, with different phase shifts between seasonal variability of extreme storms and antecedent conditions. Figure 11a presents the case with zero phase shift, i.e., where maximum rainfall and maximum runoff coefficients occur in the same month. Figure 11b presents the case for a phase shift of 3 months ($\Delta\tau = -3$) i.e., where maximum rainfall occurs three months after maximum runoff coefficients. The thick lines are the annual flood frequency curves and the thin lines are the monthly curves. The highest monthly curves in Figure 11a are for the summer months (June and July) when both highest rainfall and runoff coefficients occur. The two lines lie on top of each other as all model assumptions are strictly symmetrical around the mid of the year. The lowest monthly curves are for the winter months (December, January) where both rainfall intensities and runoff coefficients are low. For the case of a phase shift of 3 months ($\Delta\tau = -3$, i.e., maximum rain intensities in summer, maximum runoff coefficients in spring) the monthly contributions are more complex. Figure 11b shows that the monthly flood frequency curves cross over, with the probability of exceedance changing depending upon the month. The high monthly curves occur in early summer while the low curves occur in early winter. The crossing over of the monthly curves is related to the interaction of rainfall seasonality and the seasonality of antecedent soil moisture. In months with relatively wet antecedent conditions but small rainfall intensities (March, for example) small floods are quite frequent, leading to a flat flood frequency curve. In contrast, in months with relatively dry antecedent conditions and large rainfall intensities (September, for example) small floods are less frequent but a number of large floods do occur, leading to a steep flood frequency curve.

[49] In order to shed more light on this interaction of climate and catchment state seasonalities, Figure 12 shows

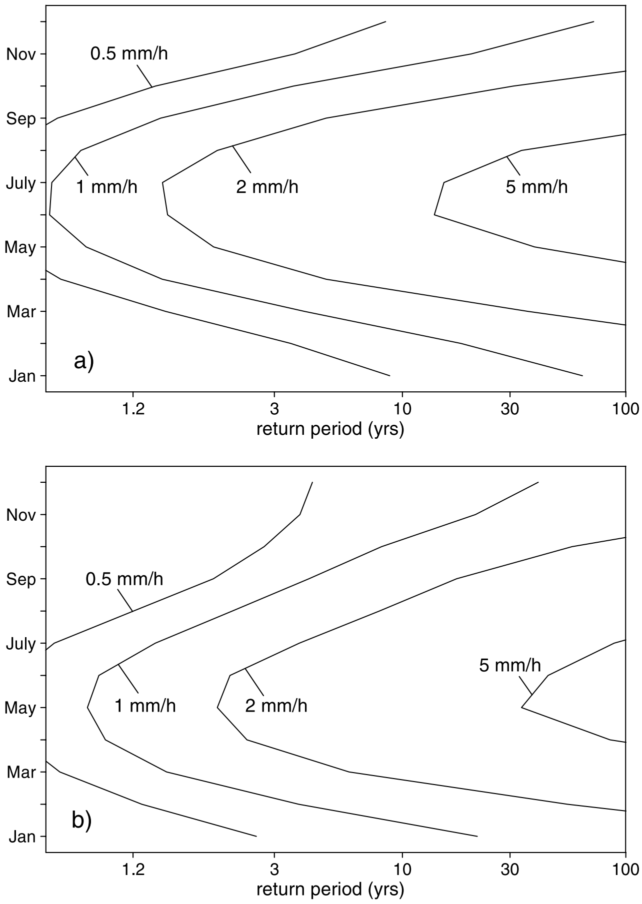

Figure 12. Probability contributions of months in terms of return period versus month for different flood peaks (0.5, 1, 2, and 5 mm/h). (a) Phase shift $\Delta\tau = 0$. (b) Phase shift $\Delta\tau = -3$ months as in Figure 11. The 1 mm/h of runoff depth is equivalent to a specific peak discharge of 0.28 $m^3/s/km^2$.

the contributions to the probability of nonexceedance from different months in terms of the return period, and for different values of the flood peak Q_p. As in Figure 11, Figure 12a presents the case for zero phase shift between extreme rainfalls and antecedent conditions $\Delta\tau = 0$ whereas Figure 12b presents the case for a three month phase shift ($\Delta\tau = -3$). Figure 12 can be thought of as slices of Figure 11 for different flood peak values (0.5, 1, 2, 5 mm/h). Figure 12 mirrors the same phenomenon exhibited in Figure 11, namely, the occurrence of extreme floods in summer, and less extreme floods throughout the year.

6. Discussion and Conclusions

[50] The paper has presented a derived flood frequency methodology that applies the theory of "mixed distributions" to account for the seasonalities of catchment state and climate forcing, and uses the χ ratio approach to incorporate the effects of within-storm patterns. Both of these advances remedy serious drawbacks in much of previous derived flood frequency research. The inclusion of seasonality and within storm time patterns change the shape of the flood frequency curve dramatically over the cases where these two aspects are ignored.

[51] The χ ratio approach is a parsimonious parameterization of the combined effect of within-storm rainfall characteristics and catchment response characteristics. Its simplicity, being a function of the ratio of storm duration and catchment response time only, makes the method amenable to analytical derivations. While the parameters given here are valid for the particular rainfall and runoff models used here, it is straightforward to derive the parameters for any rainfall and runoff model used in a particular context. For example, nonlinearity of the rainfall-runoff process will lead to higher χ ratios. More detailed investigation of the interactions of the rainfall model and the rainfall-runoff model can lead to significant improvements in the accuracy of flood estimates, and this is left for further research. The effect of the time patterns, as demonstrated here, is dramatic. As compared to the case of constant intensity rainfall, inclusion of time patterns results in almost twice the flood peak for the same return period. It is clear that the inclusion of rainfall time patterns is critically important for realistic derived flood frequency predictions and makes them more consistent with current rainfall-runoff models used in a design context.

[52] Analyses of the effects of seasonality on flood frequency indicated that indeed interannual climate variability strongly impacts upon the flood frequency characteristics in two ways, in a direct way through the seasonal variability of storm characteristics, and indirectly through the seasonality of rainfall and evapotranspiration which affect the antecedent catchment conditions for individual storm events. The relative phase shift between climate forcing and catchment state determines the magnitude and shape of the flood frequency curve. The highest impact of seasonality occurred when the seasonality in rainfall intensities was in phase with the seasonality of antecedent catchment wetness, i.e., when high rainfall intensities and large runoff coefficients occurred in the same season. This resonance increased the magnitude of the flood frequency curves by more than 50% over the case where climate forcing and catchment moisture state were out of phase. It is likely that the resonance highlighted above will be even more dramatic if the runoff generation processes were to be nonlinear, with a runoff coefficient that increases with increased rainfall. For certain combinations of the relative phase shift between climate forcing and catchment state, e.g., three months with maximum rain intensities in summer and maximum runoff coefficients in spring, the monthly flood frequency curves cross over. In months with relatively wet antecedent conditions but small rainfall intensities (March, for example) small floods are quite frequent, leading to a flat flood frequency curve. In contrast, in months with relatively dry antecedent conditions and large rainfall intensities (September, for example) small floods are less frequent but a number of large floods do occur, leading to a steep flood frequency curve. This is reminiscent of flood frequency behavior in different climates. In dry climates flood frequency curves tend to be steep while in wet climates they tend to be much flatter. This is the case in Austria. In western Austria, which is relatively wet, the CVs of the maximum annual floods are only about 0.3 while in eastern Austria which is relatively dry, the CVs of the flood frequency curves are of the order of 0.7. In

different climates around the world this contrast may be even more pronounced [see, e.g., *Iacobellis et al.*, 2002].

[53] It is interesting that any kind of seasonality (including out of phase) produces higher flood frequency curves than the case where no seasonality is included. When seasonality is present a coincidence of large runoff coefficients (wet antecedent moisture conditions) with large rainfall depths is more likely than for the case without seasonality thus producing larger flood peaks. A similar effect occurs when the runoff coefficient is allowed to vary randomly between events. When allowing for random runoff coefficients a small number of events occur where large runoff coefficients (wet antecedent moisture conditions) coincide with large rainfall depths producing very large flood peaks. The flood frequency curve not only increases on average (shifts upward), but it also increases in steepness. This is in line with the general experience that extreme floods are often produced by the combined effect of a number of factors, each of which is not particularly unusual [*Snorasson et al.*, 2002]. This is also consistent with the assessment of *Wood* [1976] on the role of random variability of model parameters in a flood frequency context.

[54] The seasonal derived flood frequency approach presented here not only allows to isolate climate versus catchment seasonalities but also to examine the probability contributions of individual months. Whereas in the observed record only one month produces the observed annual maximum flood in each year, the derived flood frequency approach can generate the relative contributions of the various months toward the annual maximum flood, i.e., the probability that the annual maximum flood of a given return period would occur in a specified month, although this cannot be verified in practice with the limited length of record currently available. For the hypothetical catchments examined here the occurrence of extreme floods is more likely in summer, and less extreme floods may occur throughout the year (Figure 12). Qualitatively, this reproduces the narrowing down in the timing of annual maximum floods with increasing return period illustrated by some of the Austrian example catchments, particularly the Teufelmühle and the Wienerbruck catchments (Figures 1a and 1c). This type of analysis facilitates the assessment of floods that occur in an unusual season. For example, a recent flood at the Salzach in Salzburg, Austria, that occurred in March 2002 [*Godina et al.*, 2003] corresponds to a return period of 100 years if only March floods are considered, while the same flood peak if it had occurred in July had been associated with a return period of only 2 years. This is very similar to the hypothetical example in Figure 12a corresponding to a flood peak of about 2 mm/h.

[55] The rainfall-runoff model used in the study is rather simple, as the main motivation is to present the generalized derived flood frequency framework, and validate it using results from the Monte Carlo approach. For applications to real catchments a more complex runoff model will likely be needed that is able to represent nonlinearities in both runoff generation and runoff routing. It is straightforward to extend the quasi-analytical framework to nonlinear models, however, equation (25) needs to be solved iteratively as in the derived flood frequency model of *Blöschl and Sivapalan* [1997], for example. It is also likely that due to the space-time intermittency of rainfall, there will be some interdependence between the contributing area of the catchment and the distributions of the duration of flood producing storms and this may also depend on the scale. Similarly, the rainfall model would have to be calibrated to each climate region of interest. These issues are left for further research.

[56] Even though the results presented here only dealt with hypothetical catchments, the results give us hope that with the proper rainfall and runoff models, we can almost fully capture the effects of seasonality in derived flood frequency models, and through these obtain valuable insights into the process controls of flood frequency. This will be extremely valuable for flood frequency regionalizations, since it enables us to regionalize individual components of the flood frequency curves (i.e., rainfall and catchment characteristics) which may be physically more meaningful than to regionalize the complete annual flood frequency curve. The results have also important implications for climate/land use change analyses. It is likely that climate change will not only impact on the flood magnitude but also on the seasonal distribution of flood occurrence. In fact, it is likely that the more obvious first indication of climate and land use change effects will be through a change in the seasonal patterns of flood occurrence. The flood frequency curve is an integrated response but we do need to isolate the controls to understand climate/land use changes and other nonstationarities.

[57] It is important to re-emphasize the purpose of this work. There have been a number of studies that have examined flood frequencies (or precipitation frequencies) separately for different seasons which were then combined into annual curves [e.g., *Buishand and Demaré*, 1990; *Rasmussen and Rosbjerg*, 1991]. These studies have generally found that separating flood frequency curves into seasons does not necessarily provide a better estimation of the annual flood frequency curve because of the larger number of parameters that need to be estimated in the case of a seasonal model. It should be noted that a better estimation of the annual flood frequency curve at gauged locations is not the main focus of this paper. The value of the proposed approach lies in the potential of isolating process controls and using known controls in a consistent way. This is in the spirit of examining and using the causative mechanisms of floods based on surface and upper weather maps of *House and Hirschboeck* [1997] and the flood process types of *Merz and Blöschl* [2003]. The method will enable hydrologists to interpret differences in observed flood frequency behavior between different climatic regions and can help to decipher climatic and catchment controls on flood frequencies, to classify variability between climatic regions, and generally to extrapolate information relating to floods from gauged to ungauged catchments.

Appendix A: Within-Storm Temporal Patterns

[58] We used explicit within-storm temporal patterns for two purposes: to estimate the χ ratio in the quasi-analytical approach, and to generate rainfall time series in the Monte Carlo approach.

[59] To define the temporal patterns of rainfall intensity for each storm we used the idea of mass curves [*Huff*,

1967; *Chow et al.*, 1988]. A normalized mass curve is defined by

$$H(t^*) = \frac{1}{i\, t_r} \int_0^t \iota(t')dt' \qquad \text{(A1)}$$

where $t^* = t/t_r$ ($0 \leq t^* \leq 1$), i is the mean rainfall intensity for the storm, $\iota(t')$ is the instantaneous rainfall intensity (within-storm pattern) at time t' internal to the storm ($0 \leq t' \leq t_r$), and t_r is storm duration.

[60] In order to generate realistic within-storm intensity patterns, we use a stochastic model capable of producing normalized mass curves satisfying the statistical characteristics described above. The model has a multiplicative structure similar to that used in random cascades. At the first level of disaggregation $H(t^*)$ is given as follows:

$$\begin{aligned} H(0) &= 0 \\ H(0.5) &= w_1 \\ H(1) &= 1 \end{aligned} \qquad \text{(A2)}$$

where w_1 is a random number with the property that $0 \leq w_1 \leq 1$. The corresponding temporal pattern consists of two rectangles of height $2w_1$ and $2(1 - w_1)$. At the next, second, level of disaggregation, the mass curve is obtained using two additional independent random variables w_2 and w_3 as follows:

$$\begin{aligned} H(0) &= 0 \\ H(0.25) &= w_1 w_2 \\ H(0.5) &= w_1 w_2 + w_1(1 - w_2) = w_1 \\ H(0.75) &= w_1 + (1 - w_1)w_3 \\ H(1) &= 1 \end{aligned} \qquad \text{(A3)}$$

[61] This corresponds to a temporal pattern with four rectangles. The disaggregation process is continued in this way to higher levels of disaggregation until the desired fine timescale (1 hour in this case) is reached. The independent random numbers $w_1, w_2, \ldots w_k, ...$ ($0 \leq w_k \leq 1$ for any k) are drawn from the beta distribution, $f_W(w)$, which is given by

$$f_W(w) = \frac{1}{B(\theta_1, \theta_2)} w^{\theta_1 - 1}(1 - w)^{\theta_2 - 1} \quad 0 < w < 1, \theta_1 > 0, \theta_2 > 0 \qquad \text{(A4)}$$

[62] When $\theta_1 = \theta_2$, $f_W(w)$ is symmetrical around $w = 0.5$, and this results in normalized mass curves the median of which is a straight line, namely the 1:1 line. The actual magnitude of $\theta_1 = \theta_2$ then controls the extent of variability around the median curve. High values of $\theta_1 = \theta_2$ give rise to smaller variability since then much of the weight of $f_W(w)$ is concentrated around $w = 0.5$. Low values of $\theta_1 = \theta_2$ cause $f_W(w)$ to be concentrated, bimodally, around $w = 1$ and $w = 0$, which causes larger variability of mass curves above and below the 1:1 line. For our purposes we chose values of $\theta_1 = \theta_2 = 1$ since the stochastically generated mass curves matched the 10%, 50% and 90% percentile mass curves estimated from data.

[63] Finally, the stochastically generated normalized mass curves are converted to within-storm temporal patterns of rainfall intensity using

$$\iota(t') = \frac{i}{\Delta}\left\{H\left(\frac{t'}{t_r}\right) - H\left(\frac{t' - \Delta}{t_r}\right)\right\} \quad t' = \Delta, 2\Delta, \ldots t_r \qquad \text{(A5)}$$

where $\iota(t')$ is the storm rainfall intensity over the period ($t' - \Delta$, t'), Δ is the time step (1 hour used in the paper), and $0 \leq t' \leq t_r$.

[64] **Acknowledgments.** This research was supported by the Austrian Science Foundation (FWF), project P14478-TEC, and the Austrian Academy of Sciences, project HÖ 18. The first author acknowledges the hospitality of Vienna University of Technology, where much of this work was completed while on his study leave. CWR reference ED 1158 MS.

References

Alila, Y., and A. Mtiraoui (2002), Implications of heterogeneous flood-frequency distributions on traditional stream-discharge prediction techniques, *Hydrol. Processes*, *16*(5), 1065–1084.

Beven, K. J. (1986), Runoff production and flood frequency in catchments of order n: An alternative approach, in *Scale Problems in Hydrology*, edited by V. K. Gupta, I. Rodriguez-Iturbe, and E. F. Wood, pp. 107–131, Springer, New York.

Blazkova, S., and K. Beven (1997), Flood frequency prediction for data limited catchments in the Czech Republic using a stochastic rainfall model and TOPMODEL, *J. Hydrol.*, *195*, 256–278.

Blöschl, G., and M. Sivapalan (1997), Process controls on regional flood frequency: Coefficient of variation and basin scale, *Water Resour. Res.*, *33*(12), 2967–2980.

Buishand, T. A., and G. R. Demaré (1990), Estimation of the annual maximum distribution from samples of maxima in separate seasons, *Stochastic Hydrol. Hydraul.*, *4*, 89–103.

Chow, V. T., D. R. Maidment, and L. W. Mays (1988), *Applied Hydrology*, McGraw-Hill, New York.

Eagleson, P. S. (1972), Dynamics of flood frequency, *Water Resour. Res.*, *8*(4), 878–898.

Fiorentino, M., and V. Iacobellis (2001), New insights into the climatic and geologic controls on the probability distribution of floods, *Water Resour. Res.*, *37*(3), 721–730.

Franks, S. W., and G. Kuczera (2002), Flood frequency analysis: Evidence and implications of secular climate variability, New South Wales, *Water Resour. Res.*, *38*(5), 1062, doi:10.1029/2001WR000232.

Godina, R., P. Lalk, P. Lorenz, G. Müller, and V. Weilguni (2003), Die Hochwasserereignisse im Jahr 2002 in Österreich, *Mitt. Hydrogr. Dienstes Oesterreich*, *82*, 1–39.

Gottschalk, L., and R. Weingartner (1998), Distribution of peak flow derived from a distribution of rainfall volume and runoff coefficient, and a unit hydrograph, *J. Hydrol.*, *208*, 148–162.

Gutknecht, D., and A. Watzinger (1996), Aufbereitung und Basisanalyse der Starkregendaten aus den Hydrographischen Jahrbüchern 1948–1993, technical report, Inst. of Hydraul., Hydrol. and Water Resour. Manage., Vienna Univ. of Technol., Vienna.

Hirschboeck, K. K. (1987), Hydroclimatically-defined mixed distributions in partial duration flood series, in *Hydrologic Frequency Modeling*, edited by V. P. Singh, pp. 199–212, Springer, New York.

Hirschboeck, K. K. (1988), Flood hydroclimatology, in *Flood Geomorphology*, edited by V. R. Baker, R. C. Kochel, and P. C. Patton, pp. 27–49, John Wiley, Hoboken, N. J.

House, P. K., and K. K. Hirschboeck (1997), Hydroclimatological and paleohydrological context of extreme winter flooding in Arizona, 1993, in *Storm-Induced Geological Hazards: Case Histories From the 1992–1993 Winter Storm in Southern California and Arizona*, edited by R. A. Larson and J. E. Slosson, *Rev. Eng. Geol.*, *XI*, 1–24.

Huff, F. A. (1967), Time distribution of rainfall, *Water Resour. Res.*, *3*(4), 1007–1018.

Iacobellis, V., P. Claps, and M. Fiorentino (2002), Climatic control on the variability of flood distribution, *Hydrol. Earth Syst. Sci.*, *6*(2), 229–237.

Jothityangkoon, C., and M. Sivapalan (2001), Temporal scales of rainfall-runoff processes and spatial scaling of flood peaks: Space-time connection through catchment water balance, *Adv. Water Resour.*, *24*(9–10), 1015–1036.

Kottegoda, N. T., and R. Rosso (1997), *Statistics, Probability and Reliability for Civil and Environmental Engineers*, 735 pp., McGraw-Hill, New York.

Kundzewicz, Z. W. (2003), Extreme precipitation and floods in the changing world, in *Water Resources Systems*, edited by G. Blöschl et al., *IAHS Publ.*, *281*, 32–39.

Merz, R., and G. Blöschl (2003), A process typology of regional floods, *Water Resour. Res.*, *39*(12), 1340, doi:10.1029/2002WR001952.

Merz, R., and G. Blöschl (2004), Regionalisation of catchment model parameters, *J. Hydrol.*, *287*, 95–123.

Merz, R., U. Piock-Ellena, G. Blöschl, and D. Gutknecht (1999), Seasonality of flood processes in Austria, in *Hydrological Extremes: Understanding, Predicting, Mitigating*, edited by L. Gottschalk et al., *IAHS Publ.*, *255*, 273–278.

Merz, R., J. Parajka, C. Reszler, and G. Blöschl (2004), Analyse regionaler Ereignisabflussbeiwerte in Österreich, technical report, Inst. of Hydraul., Hydrol. and Water Resour. Manage., Vienna Univ. of Technol., Vienna.

Mood, A. M., F. A. Graybill, and D. C. Boes (1974), *Introduction to Statistical Theory*, 3rd ed., McGraw-Hill, New York.

Ott, R. F., and R. K. Linsley (1972), Streamflow frequency using stochastically generated hourly rainfall, in *International Symposium on Uncertainties in Hydrologic and Water Resources Systems*, vol. 1, pp. 230–244, Univ. of Ariz., Tucson.

Rahman, A., P. E. Weinmann, T. M.T. Hoang, and E. M. Laurenson (2002), Monte Carlo simulation of flood frequency curves from rainfall, *J. Hydrol.*, *256*, 196–210.

Rasmussen, P. F., and D. Rosbjerg (1991), Prediction uncertainty in seasonal partial duration series, *Water Resour. Res.*, *27*(11), 2875–2883.

Robinson, J. S., and M. Sivapalan (1997a), An investigation into the physical causes of scaling and heterogeneity of regional flood frequency, *Water Resour. Res.*, *33*(5), 1045–1059.

Robinson, J. S., and M. Sivapalan (1997b), Temporal scales and hydrological regimes: Implications for flood frequency scaling, *Water Resour. Res.*, *33*(12), 2981–2999.

Sankarasubramanian, A., and U. Lall (2003), Flood quantiles in a changing climate: Seasonal forecasts and causal relations, *Water Resour. Res.*, *39*(5), 1134, doi:10.1029/2002WR001593.

Sivandran, G. (2002), Effect of rising water tables and climate change on annual and monthly flood frequencies, B. Eng. thesis, Cent. for Water Res., Univ. of West. Aust., Crawley, Australia.

Sivapalan, M., E. F. Wood, and K. Beven (1990), On hydrologic similarity: 3. A dimensionless flood frequency model using a generalized geomorphologic unit hydrograph and partial area runoff generation, *Water Resour. Res.*, *26*(1), 43–58.

Snorasson, A., H. P. Finnsdóttir, and M. E. Moss (Eds.) (2002), *The Extremes of the Extremes: Extraordinary Floods*, *IAHS Publ.*, *271*, 394 pp.

Stedinger, J. R., R. M. Vogel, and E. Foufoula-Georgiou (1992), Frequency analysis of extreme events, in *Handbook of Hydrology*, chap. 18, pp. 18.1–18.66, edited by D. R. Maidment, McGraw-Hill, New York.

Waylen, P. R., and M.-K. Woo (1982), Prediction of annual floods generated by mixed process, *Water Resour. Res.*, *18*(4), 1283–1286.

Wood, E. F. (1976), An analysis of the effects of parameter uncertainty in deterministic hydrologic models, *Water Resour. Res.*, *12*(5), 925–932.

G. Blöschl, D. Gutknecht, and R. Merz, Institute for Hydraulic and Water Resources Engineering, Vienna University of Technology, Karlsplatz 13, A-1040 Vienna, Austria. (bloeschl@hydro.tuwien.ac.at)

M. Sivapalan, Centre for Water Research, Department of Environmental Engineering, University of Western Australia, 35 Stirling Highway, Crawley, WA 6009, Australia. (sivapalan@cwr.uwa.edu.au)